Mechatronics and Making COMP0205

Final Project Report: Mechanical Design of a Lightweight Humanoid Leg

Yash Joshi — 240003413
Han Se Kendall — 240009729

08/11/2024

Contents

1 Introduction

Humanoid legs are a fundamental component in robotics and biomechanics, designed to replicate the structure and motion of human legs. Their main uses include creating legged robots and in prosthetic development. Generally, humanoid legs are designed using actuators (e.g. hydraulics) and sensors (e.g. encoders, gyroscopes). For this project, the humanoid leg under discussion will only use mechanical systems within the leg itself, involving linkages and joints. Similar to a human leg, the hip, knee and ankle joints will have their own respective mechanisms, connected by links acting as bones. Altogether, powered by a simple pulley system, the humanoid leg will act like a real human leg, with a focus on being lightweight to improve the performance characteristics of the leg, allowing for more rapid and precise movement.

1.1 Description and Function

Humanoid legs aim to imitate the behaviour and anatomy of a human leg as closely as possible, and the functions of these systems include replicating human-like motion for walking, jumping, balancing, and similar locomotive tasks. Humanoid legs are generally used for performing tasks that require dynamic movement and may be unsafe for humans to complete (e.g. rescue missions after natural disasters). We have chosen to undertake a humanoid leg system for this project in order to gain a deeper understanding in the motion of each part of the human leg, and this research could later be used in further designing legged robots and developing prosthetic legs.

In this project, we will be aiming to develop a mechanical design of a humanoid leg. This will involve modelling each of the hip, knee and ankle joints, as well as implementing mechanical linkages so that our design will replicate a human leg as closely as possible. To model the hip, knee and ankle joints, we will consider the degrees of freedom of each joint, the input angle span, the output angle span, and any other necessary variables (e.g. lengths of links).

The main desired function of our humanoid leg system will be to replicate the manner in which humans walk, and hence we will not be considering tasks such as jumping or running. We have chosen to consider walking only, because it is a vital task for all legged systems in human environments, whereas running and jumping may not be necessary in all scenarios (e.g. warehouse robots). Therefore, we have chosen this as our initial scope, with the possibility of extending the applications of the system in the future.

1.2 Industrial Uses, Research Applications, and Similar Mechanisms

One main intended use of such a humanoid leg includes creating legged robots, similar to Disney's new bipedal robot [1], which was our inspiration for this project. This robot can walk over obstacles such as wooden planks, and it can respond to human forces, in order to remain upright when being pushed. As well as this, it can walk and jump without falling and hence, this robot perfectly demonstrates the idea of dynamic balance. It does this by using a Zero Moment Point (ZMP) control algorithm, which keeps the robot's centre of mass within the support area of the feet, preventing it from toppling.

The key insights from Disney's robot is that the humanoid legs (in conjunction with

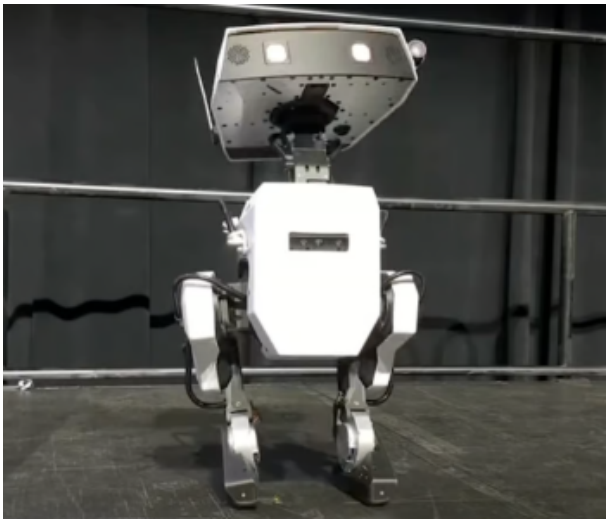

Figure 1: Disney's new bipedal robot

control algorithms) can allow it to navigate human environments, such as climbing stairs or uneven ground. For example, a system with humanoid legs could be used in disaster scenarios and rescue missions after earthquakes, to traverse unstable ground, debris and rubble. This would be unsafe for humans, so legged robots can be used in these tasks.

Figure 2: Agility Robotics' Digit: World's First Human-Centric, Multi-Purpose Robot made for Logistics Work

Another industrial use of legged robots involves using them for warehouse work as well as deliveries. An example of this is Agility Robotics' Digit robot [2], which is a bipedal robot designed to assist with lifting and moving tasks. Since warehouse work includes repetitive tasks which could cause harm to humans, this makes Digit a suitable robot for working in a warehouse. In addition, since Digit has two arms and two humanoid legs, it can move boxes and items from one place to another. Therefore, Agility Robotics have partnered with Ford to attempt using Digit for last-mile delivery, especially for tasks such as carrying packages from a vehicle to a doorstep.

Taking inspiration from Digit, similar systems with humanoid legs can be used for repetitive tasks such as warehouse work, or lifting and moving tasks such as deliveries. These robots would complete these jobs in a more efficient and accurate manner than humans, since more tasks can be executed in parallel. For example, a robot could complete one delivery while another robot completes another in a different location. Therefore, legged robots can be used in industry to work in warehouses and to deliver parcels.

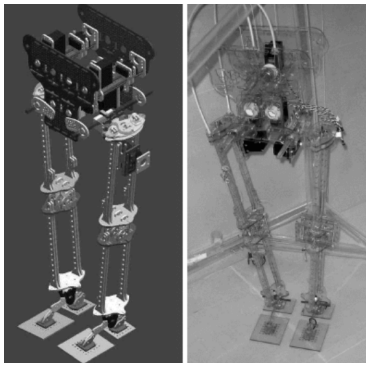

Figure 3: LARP: Light Adaptive-Reactive biPed, 3D cad assembly (left), prototype (right)

Research applications of mechanical systems with humanoid legs can be used for prosthetic development, to ensure robotic legs act exactly like human legs. One example of this research is the LARP (Light Adaptive-Reactive biPed) humanoid legged system [3], developed with the aim of understanding how natural walking motion is achieved and therefore, how it can be implemented in a prosthetic leg. To create LARP, anthropomorphic feet, knees and a mass-distribution similar to human legs were all considered, to make the model as accurate as possible. LARP has 6 degrees of freedom in each leg (same as a human leg), and the range of each joint is similar to that of humans during walking [3]. Through the LARP system, the mass-distribution of human limbs was researched, and used to create a compliant rolling-contact joint for the knee. This is a closer model of the human knee than a standard pin joint, so it provides less friction and avoids knee luxation.

Therefore, modelling the humanoid legged system exactly like a human leg can provide key insights into each joint and its properties (e.g. friction, output angle range et cetera), which can help with further prosthetic development.

1.3 Significance of this mechanism

The key criterion we are designing around is the lightweight nature of the leg. In particular, our aim is to eliminate any active actuators from the leg itself. Particularly for smaller scale bipedal applications, rapid leg motion is highly beneficial for stability and balance correction where the low inertia of the whole system make destabilisation and toppling occur much more easily and much faster. While this rapid motion can be achieved with more powerful actuators and/or transmission ratios to enhance this, this rapidly runs into a complex optimisation problem where these enhanced systems are heavier, resulting in the leg requiring more torque to accelerate and decelerate [4], requiring stronger actuators ad infinitum.

Instead, we propose a complete removal of these actuators from the leg mechanism, relying on transmission of the power of the actuator through the leg, keeping the actuators themselves in the body of the mechanism. Our approach for this is to make use of nylon cables and pulleys. We considered timing belts, but their limited flexibility rules them out, whereas the cables can be routed around corners in any direction, meaning the motion of the leg should not significantly affect them. The implementation of Bowden tubes in the system will likely be required for positioning and control consistency, and

continuous drive will not be possible due to the inherent slip in belt-like nylon cable pulley systems, as opposed to tethered systems with each end fixed to the pulleys at either end. However, we aim to set out an approach which works within these limitations, in order to implement the benefits.

Overall, this approach should significantly cut down the weight of the leg, thereby reducing its inertia and increasing its acceleration and deceleration for a given input torque. It also doesn't require a significant overall increase in weight of the whole system, other than the weight of the mechanisms and transmission which is largely negligible. This also increases the efficiency of the leg itself, reducing overall power consumption which is beneficial for autonomous robotic applications.

1.4 Mechanism Choice

We want a three degree of freedom mechanism for the hip joint for full roll-pitch-yaw control. This allows the leg to be the most versatile, particularly in static balancing and walking over rough terrain where more lateral adjustment is necessary for stabilisation. We opted for a spherical joint over a series of rotational joints as the latter has an inconsistent centre of rotation for each axis, meaning the joint doesn't rotate consistently.

With this in mind, we considered a number of typical robotic wrist mechanisms, as these often have similar sorts of motion. One was a typical robotic arm wrist, which can be modified to be cable driven through a differential mechanism [4]. This type of mechanism creates a consistent centre of rotation for the output segment, satisfying our motion criteria. However, these mechanisms can be difficult to control in small forms which is another of our criteria.

We then found another type of spherical mechanism, which has been applied both to robotic joints and also camera gimbal mechanisms, known as the spherical parallel manipulator, or SPM. However the standard configurations of this mechanism have limited rotation, which causes some issues for this use case. While limited rotation in the xz-axes (where x points forward, and z points upward relative to the body) is fine, y axis range is critical for the leg being able to complete a walk cycle. However, the range is highly dependent on the exact configuration, and in one specific case - where all three of the input axes are collinear - an assembly mode of the mechanism with infinite rotation on one axis due to the coaxial inputs is achieved [5]. Although infinite rotation is unnecessary, this has the added benefit of when turning in this axis, the output torque is the sum of the three input torques, thereby distributing the motion with the highest load across all three inputs, as opposed to only one input as is the case with other mechanisms.

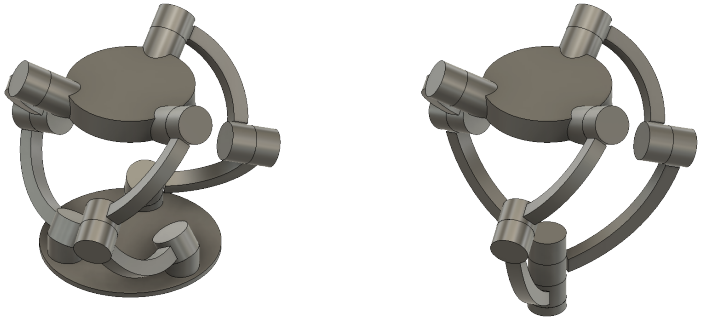

Figure 4: SPM configurations: (left) standard (right) coaxial

A notable feature of the SPM is that while the centre of rotation is fixed, the mechanism can be constructed such that the output platform rotates about that centre at any distance

- not simply rotating around the geometric centre of the platform. This is partially due to the hollow centre of the mechanism, but primarily due to the fact that the only true design constraint on the mechanics of the system is that the rotation axes of each of the three layers of joints must coincide at said rotation centre. This allows for an output platform offset away from the base such that a structural ball and socket joint could be placed within it to take loads. Inverting that, it could be offset toward the base, meaning it could be sheltered within the body of a robot, while the pivot point remains either outside of the body, or aligned with the outer wall, protecting the mechanism in more hazardous environments. This hollow centre area also means that we can run cables through the centre of this joint, down to the following joints, rather than needing complex routing.

For the knee joint, we only need a single degree of freedom. This can of course be obtained simply with a revolute joint. However, studying human knees and their motion [6], we can see that the actual path the knee joint takes is not simply rotary, but instead a combination of planar and rotary motion. More specifically, the knee first rotates around a pivot point which is travelling approximately parallel to the ground, and then later in the motion rotates around a more consistently positioned centre. Matching this in our mechanism would create a more accurate representation, and also helps propel the body forward as the leg begins to lift. This kind of motion is achievable with a cam-based joint but these can be orientation sensitive. It can also be achieved with a crossed four-bar linkage.

While this is critical for prosthetic and prosthetic research applications, it is not strictly necessary in purely robotic applications. These do not need to perfectly match the motion of human legs - only parallel it. However, these linkages do offer some other benefits in these cases. For one, it provides a variable input to output ratio. This means the mechanism can be tuned to give the desired performance characteristics, such as the joint moving slower at the beginning of its motion, where there is high load, and faster at the end where this is not necessary. We also considered a crank-rocker mechanism which would allow for continuous motion to drive the joint, rather than requiring reversible motion. This improves the overall efficiency of the motion, and simplifies control as discussed in [7] which seeks to create a quadrupedal system consisting of four legs each with only one degree of freedom. This concept was impractical for our case however, since the requirement for a cable-driven system rules out continuous rotation transmission, at least for high torque cases, as cables are highly prone to slip when unanchored as would be necessary for continuous rotation. Therefore, we settled on the four-bar linkage as the mechanism for the knee.

For the ankle joint, a worm gear driven four-bar linkage has been chosen for two main reasons. Firstly, a worm-drive prevents back-driving of the foot, since it bears the full weight of the foot, and this is beneficial because it ensures the foot remains stable both when static and while in motion. In addition, the worm gear can be cable driven, even with multiple rotations, by wrapping the cable around the pulley more than once, unlike other significant torque increase mechanisms. This enables continued use of the cable-drive approach to meet our criteria of weight. Secondly, the four-bar again allows for variable gear ratios and a non-circular revolution. The crossed element is unnecessary here, as the higher mechanical advantage ranges are not needed due to the worm-spur gear train, so instead a standard four-bar is used.

Contrary to a real human leg, we will model the ankle joint as a 1 Degree of Freedom (DoF) joint rather than a 2 DoF joint for mechanical simplicity. In addition, the primary function of the ankle during walking (our chosen task) only involves flexing up and down, so 1 DoF can easily cover the tasks needed to maintain a straight walking gait.

2 Mathematical Modelling

In modelling this system, we take the approach of breaking down the leg into three subsystems, defining transformation matrices and offset vectors between the hip, knee, and ankle. These matrices then allow for the individual mechanisms to be combined into a single model. Additionally, this subsystem-based approach allows any of the three mechanisms to be reused for other applications, or replaced with alternatives in the future. It also helps with easy parametrisation since considering each system individually is much simpler.

2.1 Hip Joint

The methods for solving forward kinematics of general SPMs are fairly well established [8]. The inverse kinematics for the coaxial variant are more complicated due to the infinite rotation element, but we do not need to consider these at this point. The kinematics of the mechanism is most easily modelled in terms of the joint vectors rather than in terms of lengths and points, so we start by defining three sets of normalised vectors - $\hat{\boldsymbol{u}}_{\boldsymbol{i}}$,$\hat{\boldsymbol{v}}_{\boldsymbol{i}}$ and $\hat{\boldsymbol{w}}_{\boldsymbol{i}}$ - for $i = [1, 2, 3]$. All of these vectors are directed outward from the origin about which the output platform of the mechanism rotates. The $\hat{\boldsymbol{u}}_{\boldsymbol{i}}$ vectors are the vectors through the base joints of each proximal link. In our case of a coaxial SPM, we can use a simplification [5] where $\hat{\boldsymbol{u}}_{\boldsymbol{i}}=[0, 0, -1]^{\boldsymbol{T}}$. The $\hat{\boldsymbol{w}}_{\boldsymbol{i}}$ vectors and $\hat{\boldsymbol{v}}_{\boldsymbol{i}}$ vectors are the vectors through the joints between the proximal and distal links, and the distal links and output platform respectively. These are the joints we need to solve for to determine the arrangement of the mechanism for given input values of θ_i.

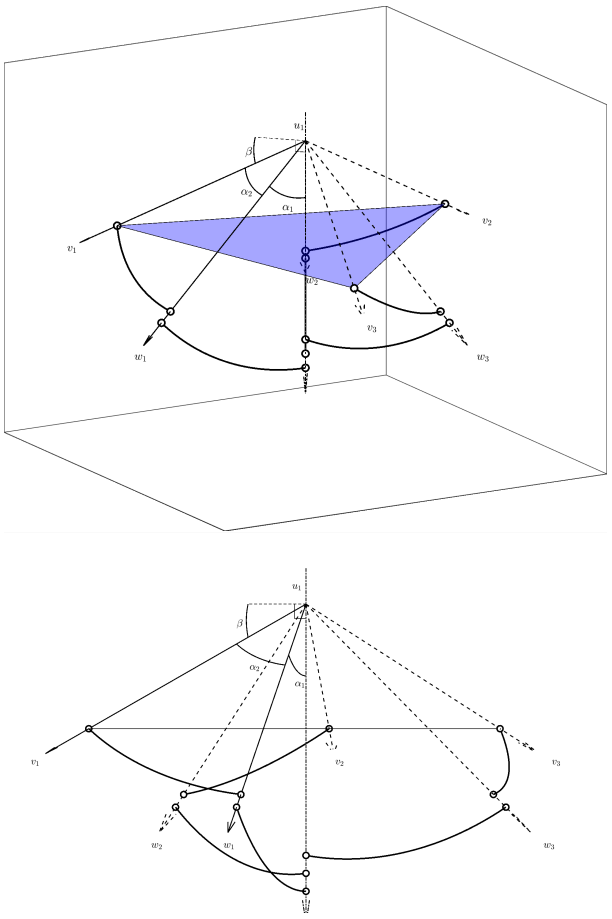

Figure 5: Schematics of the SPM model

To characterise the mechanism, we use three defining angles - α_1, or the angle between the $\hat{\boldsymbol{u}}$ and $\hat{\boldsymbol{w}}$ vectors, α_2, or the angle between the $\hat{\boldsymbol{w}}$ and $\hat{\boldsymbol{v}}$ vectors, and β, or the angle between the $\hat{\boldsymbol{v}}$ vectors and the horizontal plane when the mechanism is in its home configuration. The $\hat{\boldsymbol{w}}$ vectors are easily

definable in terms only of the input argument $\theta = [\theta_1, \theta_2, \theta_3]$.

$$\hat{\boldsymbol{w}}_{\boldsymbol{i}} = \begin{bmatrix} \sin(\eta_i - \theta_i)\sin\alpha_1 \\ \cos(\eta_i - \theta_i)\sin\alpha_1 \\ -\cos\alpha_1 \end{bmatrix} \tag{1}$$

$$\eta_i = \frac{2(i-1)\pi}{3} \tag{2}$$

This definition then leads us to the following system, using the characterising angles

$$\begin{cases} \hat{\boldsymbol{w}}_{\boldsymbol{i}} \cdot \hat{\boldsymbol{v}}_{\boldsymbol{i}} = \cos\alpha_2 & i = [1,2,3] \\ \hat{\boldsymbol{v}}_{\boldsymbol{i}} \cdot \hat{\boldsymbol{v}}_{\boldsymbol{j}} = \cos\alpha_3 & i,j = [1,2,3]; i \neq j \\ ||\hat{\boldsymbol{v}}_{\boldsymbol{i}}|| = 1 & i = [1,2,3] \end{cases} \tag{3}$$

$$\alpha_3 = 2\arcsin\left(\sin\beta\cos\tfrac{\pi}{6}\right) \text{ (The angle between adjacent } \hat{\boldsymbol{v}}_{\boldsymbol{i}} \text{ vectors)} \tag{4}$$

Taking this definition, we obtain a system of nine non-linear equations for the nine unknowns we have, giving us a perfectly constrained system albeit one which must be solved numerically. However, this set of nine equations signifies that we do also have eight possible configurations for any given set of input angles. This is due to each of the proximal-distal link pairs being able to be in a left-hand or right-hand state (i.e. the distal link can point either to the left or right of the proximal link it is attached to). The schematic provided has a right-right-right (or rrr) configuration, however any permutation of right-handed and left-handed states is valid (see figure 6). This gives us a physical explanation for the number of solutions, but still presents some issues. Namely, the physical links cannot instantaneously shift between left-handed and right-handed configurations (except when they reach a parallel state).

To prevent this from becoming a problem in simulation, we use the signs of the $\hat{\boldsymbol{v}}_{\boldsymbol{i}}$ vectors at the home position of the system as the initial guess for the solver. This maintains the simulation in the correct configuration, except for when the system is spun about the z-axis such that $|\theta_i| > 60^\circ \quad \forall\ 1 \leq i \leq 3$.

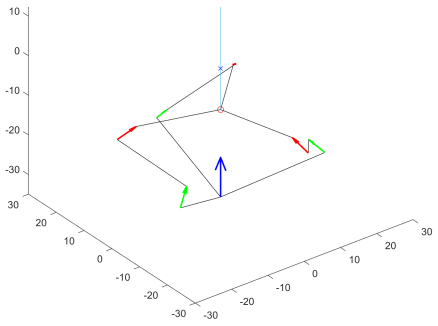

Figure 7: Chosen SPM configuration

We selected the configuration shown in figure 7 with $\boldsymbol{\alpha_1 = 45^\circ}$, $\boldsymbol{\alpha_2 = 40^\circ}$, and $\boldsymbol{\beta = 62.345^\circ}$. This places the output platform below the centre of origin (shown with an x in the plot). This allows the leg itself to be offset so it is clear of the links, and have the leg pivot around the correct point. If this arrangement proves too weak to support the weight of the leg, we can flip the offset and introduce a load-bearing ball and socket joint between the base plate and end effector, reducing the static load on the links.

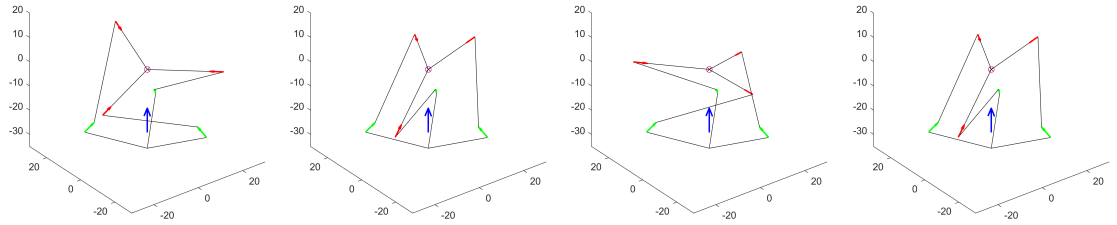

(a) l-l-l configuration (b) l-l-r configuration (c) l-r-l configuration (d) l-r-r configuration

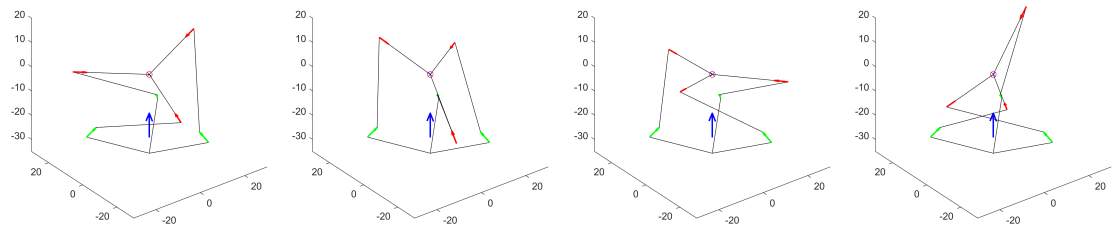

(e) r-r-r configuration (f) r-r-l configuration (g) r-l-r configuration (h) r-l-l configuration

Figure 6: The eight configurations of an SPM model (not the same one as we selected), for $\theta = [65°, 75°, 90°]$

2.2 Knee Joint

In modelling, the crossed element of the four-bar linkage prevents easy application of the usual trigonometric methods for solving a standard four-bar linkage. Instead, we take a vector approach, resolving each of the links. This requires us defining one extra angle - γ - to allow us to resolve the top linkage into its components.

$$\begin{bmatrix} C\cos\alpha - B\cos\gamma \\ C\sin\alpha + B\sin\gamma \end{bmatrix} = \begin{bmatrix} A - D\cos\theta \\ D\sin\theta \end{bmatrix} \tag{5}$$

$$\gamma = \arccos\left(\frac{C\cos\alpha + D\cos\theta - A}{B}\right) = \arcsin\left(\frac{D\sin\theta - C\sin\alpha}{B}\right) \tag{6}$$

Combining these, and applying the identity $\mathbf{\sin(\arccos\theta) = \sqrt{1-\theta^2}}$ we can eliminate γ and begin simplifying.

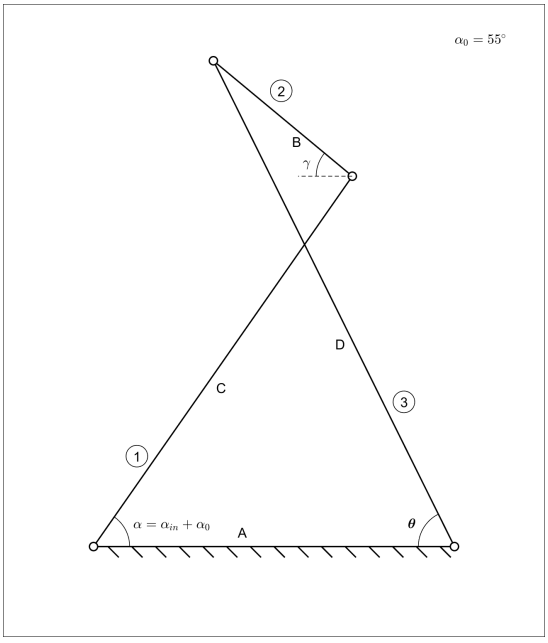

Figure 8: Schematic of a crossed four-bar

$$\sin\left(\arccos\frac{C\cos\alpha+D\cos\theta-A}{B}\right)=\frac{D\sin\theta-C\sin\alpha}{B} \tag{7}$$

$$\sqrt{1-\left(\frac{C\cos\alpha+D\cos\theta-A}{B}\right)^2}=\frac{D\sin\theta-C\sin\alpha}{B} \tag{8}$$

$$1-\left(\frac{C\cos\alpha+D\cos\theta-A}{B}\right)^2=\left(\frac{D\sin\theta-C\sin\alpha}{B}\right)^2 \tag{9}$$

$$B^2-A^2-C^2(\cos^2\alpha+\sin^2\alpha)-D^2(\cos^2\theta+\sin^2\theta)+2AC\cos\alpha = 2D(C\cos\alpha-A)\cos\theta-2DC\sin\alpha\sin\theta \tag{10}$$

Using the identity $\boldsymbol{a\cos\theta+b\sin\theta=R\cos(\theta-x)}$ where $\boldsymbol{R=\sqrt{a^2+b^2}}$ and $\boldsymbol{x=\arctan\left(\frac{b}{a}\right)}$, we can simplify this equation to a single term in θ which can then be rearranged to form the equation for θ we are looking for. To shorten the written equation, and reduce repeat calculations for simulation purposes, we make the following statements.

Let

$$k=\frac{B^2-A^2-C^2-D^2+2AC\cos\alpha}{2D}$$
$$a=C\cos(\alpha)-A$$
$$b=-C\sin(\alpha)$$

We then get

$$k=\sqrt{a^2+b^2}\cos\left(\theta-\arctan\left(\frac{b}{a}\right)\right) \tag{11}$$

$$\frac{k}{\sqrt{a^2+b^2}}=\cos\left(\theta-\arctan\left(\frac{b}{a}\right)\right) \tag{12}$$

$$\theta=\arccos\frac{k}{\sqrt{a^2+b^2}}+\arctan\left(\frac{b}{a}\right) \tag{13}$$

Now that we have an equation for θ in terms of α, we can easily determine the position of the mechanism for any given input angle, and thereby characterise the overall motion of the system, including trajectory and output direction, for which we consider the angle of link **2** to the x-axis. This allows simpler calculation for characterisation of the overall angle range. Then, for the final configuration, the leg can be attached at the angle which provides the desired initial angle for the leg.

Using two set parameters - $\boldsymbol{A=20}$ and $\boldsymbol{B=10}$ - we obtain the following plots for the ranges $\boldsymbol{10<C<60}$ and $\boldsymbol{20<D<50}$.

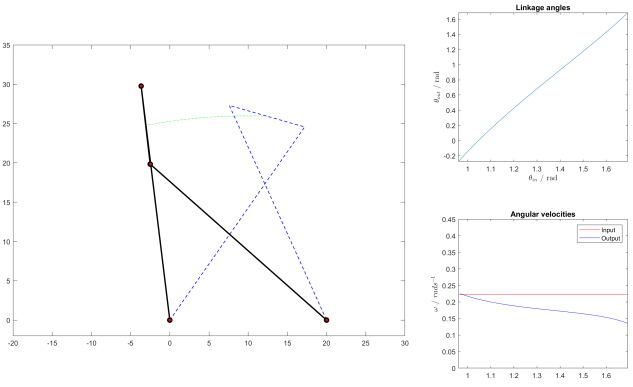

Figure 9: Unstable state

The necessary range of motion for the knee joint during a walk cycle is around 60°-70°[9], although the total range is around 135° so we decided to aim for between 130° and 140°. When selecting the parameters, we also needed to watch for the cases where the mechanism went to a physical limit, where the linkage unfolds into a triangle consisting of links $\boldsymbol{1,2+3,4}$.

In these cases, although an arrangement might seem to have the range we wanted, if the mechanism reached a physical limit at the end of its motion, the effective limit would actually be lower. This is due to the linkage becoming unstable as it tends towards this limit, particularly as it passes through the state where the angle between links 2 and 3 is zero (see figure 9). At this point, external loads are transmitted very awkwardly through the mechanism, putting significant torques on the each of the base joints, and especially the driving joint.

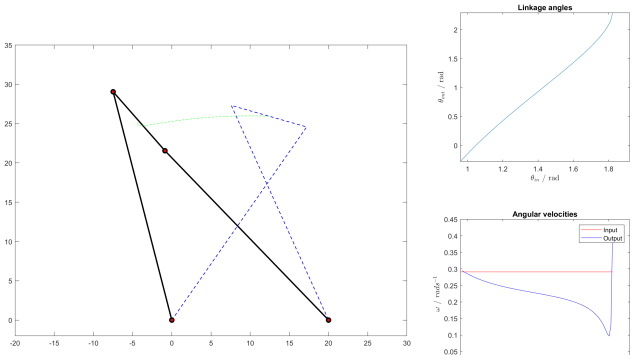

Figure 10: Simulation "end state", beyond unstable state

These can be seen on the plots as output angle plots which end before the maximum angle for θ_{in} $\left(\frac{2\pi}{3}\right)$. These configurations can still be used - they simply take a smaller range of θ_{in}. The output angle plots which start at $\theta_{in} > 0$ are also still valid, they again have a smaller range, as the initial angle is greater.

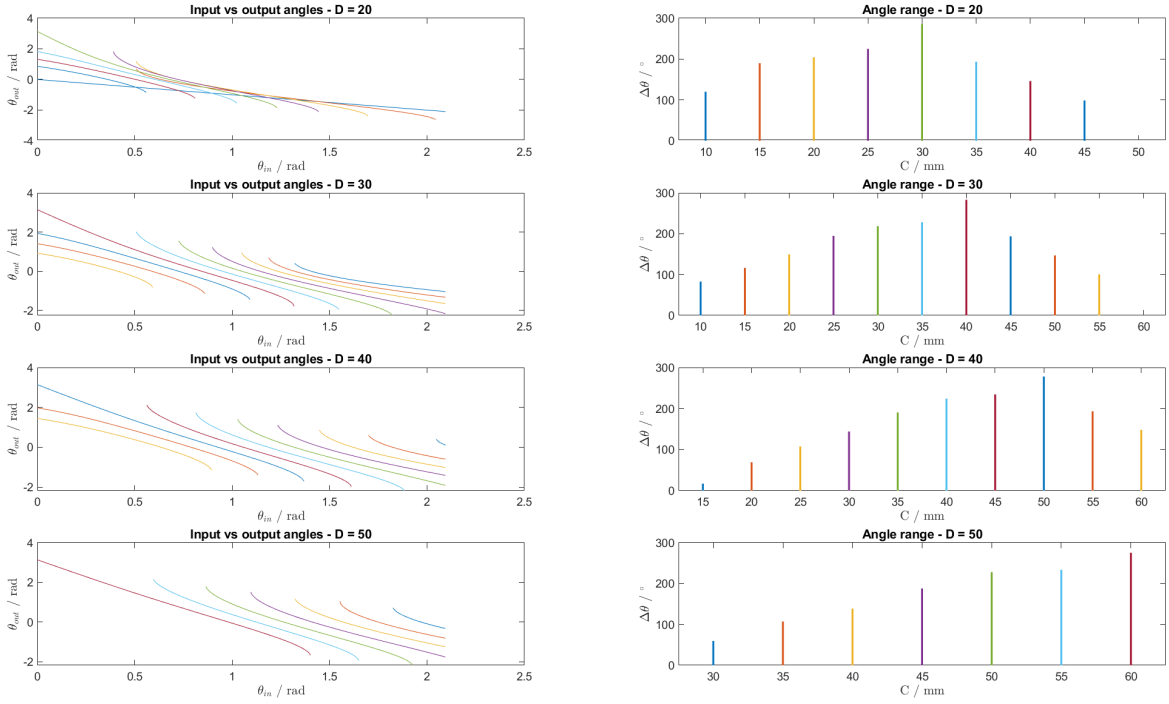

Figure 11: Crossed 4-bar parametrisation; links C and D

We also varied $\boldsymbol{B}$ and $\boldsymbol{C}$ while maintaining $\boldsymbol{A = 10, D = 20}$, to compare it to the first plot and understand the effect B has on the overall trajectory (see figure 12). For all of these, the important factor in trajectory and angular velocity is the ratio of lengths.

Note that where we see a starting point for a path for which $\theta_{out} + \theta_{in} < 0$, the system is starting unfolded in a zig-zag configuration (figure 13), so we dismiss these cases. There are some other conditions for which this is true, but these can be considered case-by-case.

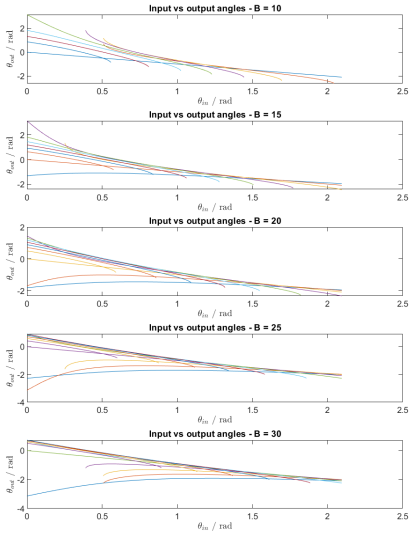

Figure 12: Crossed 4-bar parametrisation; links B and C

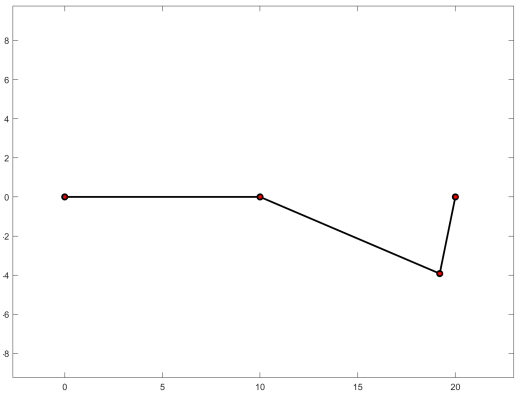

Figure 13: Invalid zig-zag initial configuration

Overall, we can see that as $\boldsymbol{B}$ tends towards the value of $\boldsymbol{A}$, the spread of the angular ranges decreases, giving us less options for the parametrisation. However, the further away it gets, the less stable the paths are, with much shorter input angle ranges. Therefore, we ended up settling on $\boldsymbol{B = 20, C = 25, D = 30}$, giving us the ratio $\boldsymbol{A : B : C : D}$ as being $1 : 0.5 : 1.25 : 1.5$. This gives us a starting angle of $\theta_{in} \approx 0.91$, and provides an output range of $-1.03 < \theta_{out} < 1.71$, or a total range of 156°.

This is considerably more than the 135° we were targeting. However, at its starting position, the rate of change of θ_{out} with respect to θ_{in} is large, making this part unsuitable for use as it has a low effective gear ratio, thereby reducing the load the leg can hold. Therefore, we decided to leave the first 0.15 radians of the range unused, cutting the effective range down by 20°and reducing this zone of mechanical disadvantage.

We cannot completely eliminate this zone without cutting the output range down too low or needing to significantly increase the input range, even using other arrangements. The solution is to invert the mechanism, using the maximum value of θ_{in} as the starting position. This aligns the range of θ_{in} for which we have the greatest mechanical advantage with the configuration of the leg which was under the most load. Our current concern is static loading, since this configuration will not have the same geometrical advantage as the default start position in terms of compressive strength when the leg is straight and static. However, the mechanical advantage present should make it be still practical to hold the joint in this position.

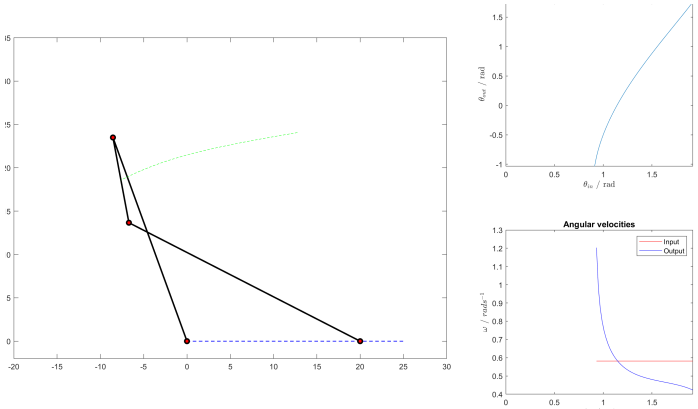

Figure 14: Selected crossed four-bar lengths

2.3 Ankle Joint

In this model, while bars A and B are imaginary, and bars C and D physically exist, the mechanism is still a four bar linkage, and can be modelled as such. As shown in the schematic diagram, the ends of bar A are fixed, and one end of bar B is fixed with the other one lying on the spur gear. As an additional stage, the angular velocity of the worm gear defines the angular velocity of the spur gear, which hence the input angle for the four-bar is simply linearly dependent on the input angle of the worm gear. Combining these together, the resultant mechanism model is a worm gear driven four-bar linkage.

Contrary to the standard four-bar linkage, in this mechanism, bar B cannot spin in a full circle due to the length constraints of bars C and D, and this makes the linkage a more accurate model of the human ankle joint. Therefore, similar to the knee joint, this added constraint prevents easy application of the usual trigonometric methods for solving a standard four-bar linkage.

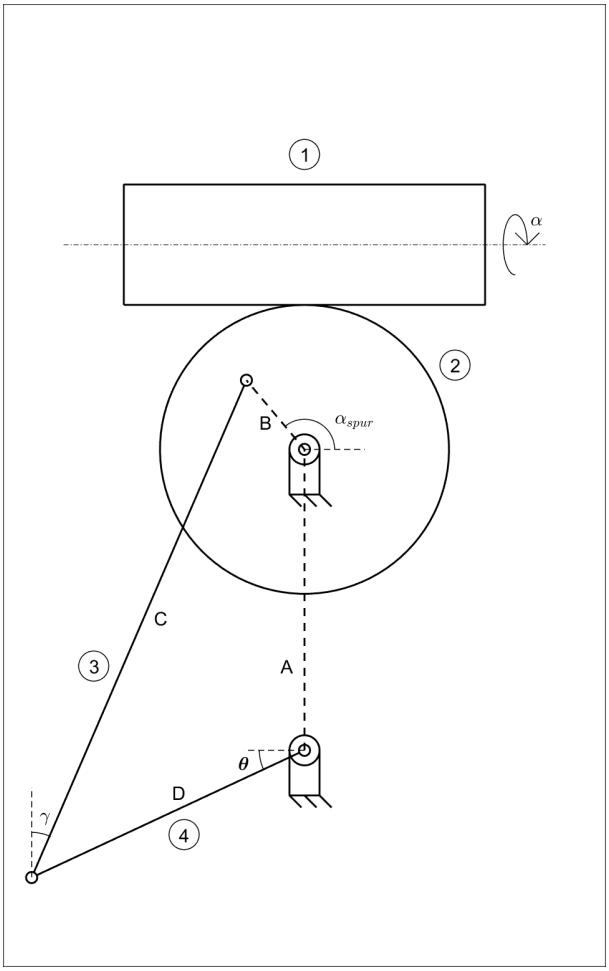

Figure 15: Schematic of a worm gear driven four-bar

Instead, we take a vector approach, resolving each of the links. This requires us defining one extra angle - γ - to allow us to resolve the top linkage into its components - however this can be eliminated again later when combining the equations.

$$\begin{bmatrix} C\sin\gamma - B\cos\alpha_{spur} \\ C\cos\gamma - B\sin\alpha_{spur} \end{bmatrix} = \begin{bmatrix} D\cos\theta \\ A + D\sin\theta \end{bmatrix} \tag{14}$$

$$\gamma = \arccos\left(\frac{A + D\sin\theta + B\sin\alpha_{spur}}{C}\right) = \arcsin\left(\frac{D\cos\theta + B\cos\alpha_{spur}}{C}\right) \tag{15}$$

Combining these, and applying the identity $\mathbf{\sin(\arccos\theta) = \sqrt{1-\theta^2}}$ we can eliminate γ and begin simplifying.

$$\sin\left(\arccos\frac{A+D\sin\theta+B\sin\alpha_{spur}}{C}\right)=\frac{D\cos\theta+B\cos\alpha_{spur}}{C} \tag{16}$$

$$1-\left(\frac{A+D\sin\theta+B\sin\alpha_{spur}}{C}\right)^2=\left(\frac{D\cos\theta+B\cos\alpha_{spur}}{C}\right)^2 \tag{17}$$

$$\begin{aligned}C^2-A^2-B^2(\cos^2\alpha_{spur}+\sin^2\alpha_{spur})-\\ D^2(\cos^2\theta+\sin^2\theta)-2AB\sin\alpha_{spur}\end{aligned}=\begin{aligned}&2BD\cos\theta\cos\alpha_{spur}+2AD\sin\theta+\\ &2BD\sin\theta\sin\alpha_{spur}\end{aligned} \tag{18}$$

As before, using the identity $\boldsymbol{a\cos\theta+b\sin\theta=R\cos(\theta-x)}$ where $\boldsymbol{R=\sqrt{a^2+b^2}}$ and $\boldsymbol{x=\arctan\left(\frac{b}{a}\right)}$, we can simplify this equation to a single term in θ. For clarity, we make the following statements.

Let

$$k=\frac{C^2-A^2-B^2-D^2-2AB\sin\alpha_{spur}}{2D}$$

$$a=B\cos\alpha_{spur}$$

$$b=A+B\sin\alpha_{spur}$$

This then gives us

$$k=\sqrt{a^2+b^2}\cos\left(\theta-\arctan\left(\frac{b}{a}\right)\right) \tag{19}$$

$$\frac{k}{\sqrt{a^2+b^2}}=\cos\left(\theta-\arctan\left(\frac{b}{a}\right)\right) \tag{20}$$

$$\theta=\arccos\frac{k}{\sqrt{a^2+b^2}}+\arctan\left(\frac{b}{a}\right) \tag{21}$$

We can then go through the same process as we did for the knee joint, parametrising the mechanism with $\boldsymbol{A=5}$ and $\boldsymbol{B=15}$ held constant and choosing a configuration which has the desired characteristics (figure 17). These were around a 60° range, and a mostly linear relationship between the input and output angles. We decided on the angle by considering human biology, and the linear relationship due to the transmission already providing the necessary torque, so linear travel would be easier to work with as well as meaning the foot would have consistent load-bearing capability throughout its motion, allowing for more complex walk cycles or even run cycles, where the foot would be load bearing in its pointed configuration.

Based on this, we decided on lengths of $\boldsymbol{C=90, D=50}$ giving us the ratio $\boldsymbol{A:B:C:D}$ as $1:0.3:1.8:1$. This gives a 57.2° range, and a close to linear output ratio due to the rotation being constrained to a limited segment of the spur gear. For the modelled gear ratio of $\frac{1}{24}$ between the worm and spur gears, a total input of 6 rotations is required to realise this motion.

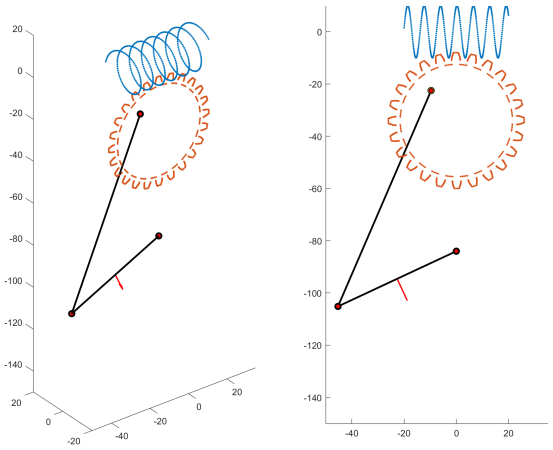

Figure 16: Worm gear driven ankle model

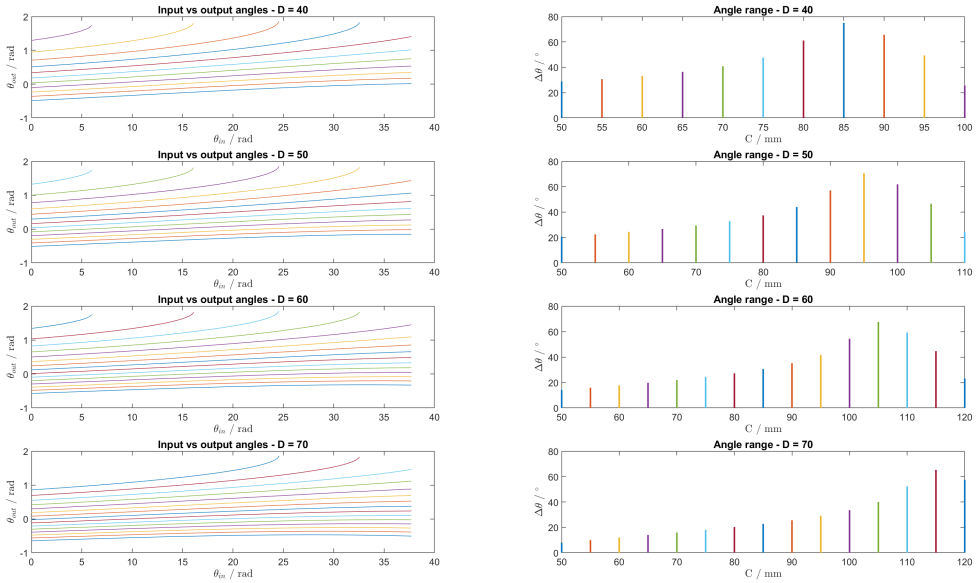

Figure 17: Worm gear driven four-bar parametrisation; links C and D

2.4 Model combination

To model the mechanism, we now need to establish rotation matrices which transform points from the input coordinate frame to the output coordinate frame of each stage of the leg, as well as offset vectors for the start to the end of the mechanism. For both the knee and ankle joints, these are simply rotations about the z-axis (as both are modelled in the xy-plane) by the angle θ_{out}, and are therefore in the form of basic rotation matrices. Their offset vectors are also simply the position vector of their defined output point, as both were modelled with their base position at the origin. This vector is then multiplied by the input transformation matrix, which defined how that mechanism was oriented to obtain it in the global frame.

$$R_{output} = R_{input} \begin{bmatrix} \cos\theta_{out} & -\sin\theta_{out} & 0 \\ \sin\theta_{out} & \cos\theta_{out} & 0 \\ 0 & 0 & 1 \end{bmatrix} \tag{22}$$

$$\boldsymbol{v}_{output} = R_{input}\boldsymbol{p} \tag{23}$$

The transformation defined by the SPM is more complicated due to it having three degrees of freedom. However, the output platform's transformation from its initial position ($\theta = [0, 0, 0]$) can be broken down into Euler angles, and then recombined into a single transformation matrix by multiplying the individual matrices associated with each angle. The mechanism is defined in its default state as having the coaxial input lying normal to the xy plane, and its output platform parallel to said plane, as visible in figure 7.

Let

$\hat{\boldsymbol{n}}$ = (The current platform normal)

$\hat{\boldsymbol{n}}_{\boldsymbol{0}}$ = (The platform home position normal, or local z axis)

$\hat{\boldsymbol{v}}$ = (The direction vector between the platform centre and joint with link 1)

$\hat{\boldsymbol{v}}_{\boldsymbol{0}}$ = (As above, for the home position)

$\hat{\boldsymbol{a}}_{\boldsymbol{rot}} = \hat{\boldsymbol{n}} \times \hat{\boldsymbol{n}}_{\boldsymbol{0}}$ (The axis of rotation for pitch)

We obtain

$$\theta = \arccos(\hat{\boldsymbol{n}} \cdot \hat{\boldsymbol{n}}_{\boldsymbol{0}}) \tag{24}$$

$$\psi = \begin{cases} 0 & \theta \approx 0 \\ -\arccos(\hat{\boldsymbol{v}} \cdot \text{Rotate}(\hat{\boldsymbol{v}}_{\boldsymbol{0}}, \hat{\boldsymbol{a}}_{\boldsymbol{rot}}, \theta)) & \text{default} \end{cases} \tag{25}$$

$$\phi = \begin{cases} -\arccos(\hat{\boldsymbol{v}} \cdot \text{Rotate}(\hat{\boldsymbol{v}}_{\boldsymbol{0}}, \hat{\boldsymbol{a}}_{\boldsymbol{rot}}, \theta)) & \theta \approx 0 \\ \arccos(\hat{\boldsymbol{v}} \cdot \hat{\boldsymbol{a}}_{\boldsymbol{rot}}) & \text{default} \end{cases} \tag{26}$$

$$R = \begin{bmatrix} \cos\phi & -\sin\phi & 0 \\ \sin\phi & \cos\phi & 0 \\ 0 & 0 & 1 \end{bmatrix} \begin{bmatrix} 1 & 0 & 0 \\ 0 & \cos\theta & -\sin\theta \\ 0 & \sin\theta & \cos\theta \end{bmatrix} \begin{bmatrix} \cos\psi & -\sin\psi & 0 \\ \sin\psi & \cos\psi & 0 \\ 0 & 0 & 1 \end{bmatrix} \tag{27}$$

Note that in simulation, some correction for discontinuities when angles exceed 2π, or sin/cos ambiguities is required, particularly for ϕ.

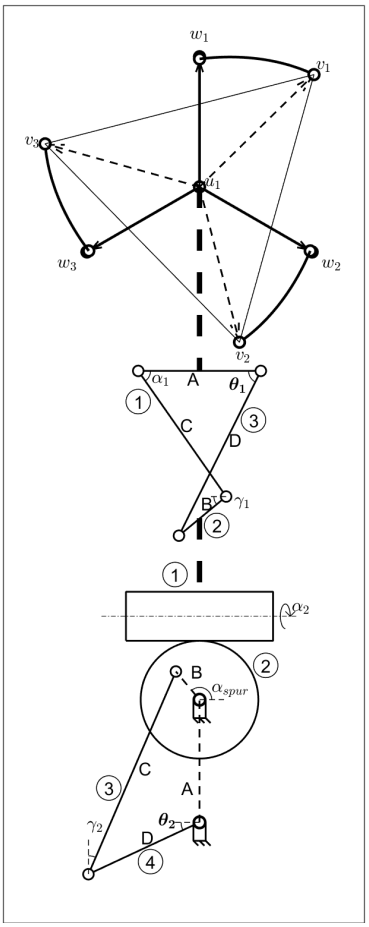

Figure 18: Full schematic diagram

Using the defined transformation matrices, offsets and length constants for the distances between each joint, we can obtain a complete model for the leg, driven by 5 angular inputs. In the form of a MATLAB program, this provides an output such as that shown below in figure 19.

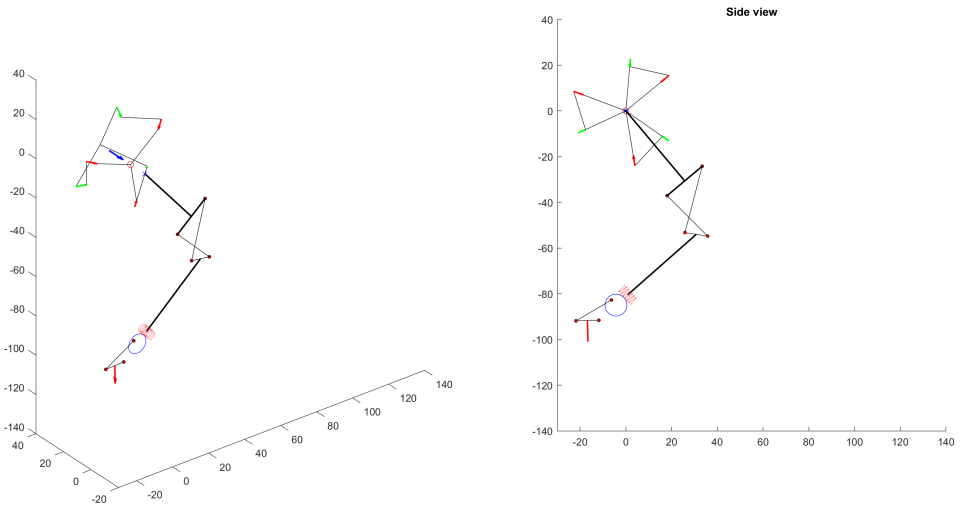

Figure 19: MATLAB simulation combining all three models

3 Mechanical Analysis

3.1 Mechanical System Overview

As shown above in figure 19, the hip and the knee, as well as the knee and the ankle are joined together by solid links, which act as bones (femur and tibia respectively), in order to form the complete shape of human leg. This results in a mechanical system (figure 19) which contains:

- 5 overall Degrees of Freedom:
  - Hip joint: 3 - the SPM joint allows for rotation around the x, y and z axes
  - Knee joint: 1 - the crossed four-bar linkage only allows for rotation around 1 axis
  - Ankle joint: 1 - the worm gear driven four-bar linkage only allows for rotation around 1 axis, same axis as the knee joint
- 12 overall links:
  - Hip joint: 7 - the SPM model uses 3 proximal links, 3 distal links and 1 link at the end effector
  - Knee joint: 3 - the crossed four-bar uses 3 physical bars and the fourth bar is part of the SPM end effector, so is not counted separately.
  - Ankle joint: 2 - the worm gear driven four bar uses 2 physical bars (as shown in figure 15), and the other 2 bars are imaginary
- 18 overall mechanical joints:
  - Hip joint: 9 - the SPM model uses 3 proximal joints, 3 distal joints, and 3 joints along the central axis. All of these joints are revolute joints
  - Knee joint: 4 - the crossed four-bar uses 4 joints at the ends of the bars (as shown in figure 8). All of these joints are revolute joints
  - Ankle joint: 5 - the worm gear driven four-bar uses 4 joints at the ends of the bars, and another joint between the worm gear - spur gear assembly. All of these joints are revolute joints

We will be using a simple pulley system to power the hip joint, which in turn will drive the knee joint, which will drive the worm gear in the ankle joint. The worm gear will then cause the spur gear to rotate, and hence the foot will bend accordingly. The torque needed to power the overall system will depend on the final link lengths. The gear ratio between the worm gear - spur gear assembly is $\frac{1}{24}$, since the spur gear will have 24 teeth.

Other considerations to mechanism parts and implications of varying mechanism features are:

- In the SPM model for the hip joint, all proximal links and all distal links must have the same lengths to ensure the end effector's position lies in the centre of the model
- The link A in the crossed four-bar in the knee must be perpendicular to the link between the hip and the knee (as shown in figure 19) to ensure the knee's motion

replicates a human knee

- The axis of rotation of the worm gear must be parallel to link A in the knee, to ensure the ankle's motion replicates a human ankle
- As the lengths of any links increase, the total weight of the whole mechanical system will also increase, so the torque needed to move all joints will be larger
- As the lengths of bars C and D increase in the crossed four-bar, the output angle θ will also be larger for the same input angle α, due to equation 13. This means the output angle range will be larger, and the angular velocity of the effector will increase.
- As the lengths of bars C and D decrease in the ankle joint, the output angle θ will be larger for the same input angle α_{spur}, due to equation 21. This means the output angle range will be larger, and the angular velocity of the foot will increase.

3.2 Angle Constraints and Overall Span

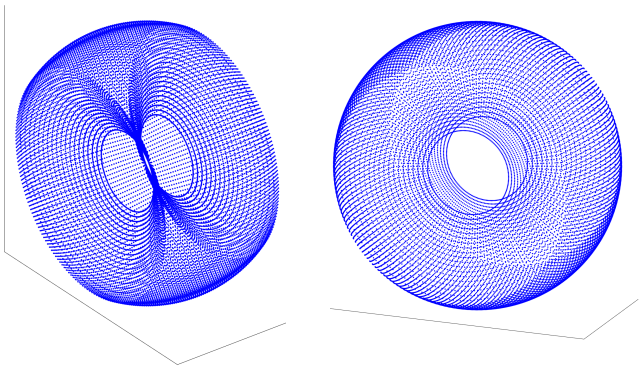

Figure 20: Angle range

The safe range of motion for the hip joint is approximately $\pm 30°$ around the x and z axes, and infinite around the y axis. When the knee and ankle bends, it simply shortens the overall length of the leg, as both joints are planar, so the range remains within the same volume. This produces a range plot (figure 20) which is essentially a sphere of radius x (the extended leg length), and with two spherical sectors removed, each cap of height $x(1 - \sin\frac{\pi}{6})$. Additionally, another concentric sphere of radius equal to shortest configuration of the leg (where the knee is fully bent) is also removed.

The leg only practically needs to move in the lower segment of this plot, with the SPM y-axis output rotation ranging between -10° and 110°. The knee input angle then varies between 0° and 60° providing an output angle range of 136°. Finally the ankle input angle varies between 0° and 2160° (6 rotations of the worm gear) for an output range of 57.2°.

References

[1] L. Blain. *Disney's super-cute new bipdeal robot demonstrates the power of style*. URL: https://newatlas.com/robotics/disney-wall-e-robot/. accessed: 08.10.2024.

[2] *Agility Robotics Digit Patents: Humanoid Robot*. URL: https://insights.greyb.com/agility-robotics-digit/.

[3] Giuseppina Gini, Umberto Scarfogliero, and Michele Folgheraiter. *Human-Oriented Biped Robot Design: Insights into the Development of a truly Anthropomorphic Leg*. 2007. accessed: 05.11.2024.

[4] V. P. Nguyen et al. *Low-Cost Cable-Driven Robot Arm with Low-Inertia Movement and Long-Term Cable Durability*. URL: https://www.mdpi.com/2218-6581/13/9/128. accessed: 10.10.2024.

[5] I. Tursynbek, A. Niyetkaliyev, and A. Shintemirov. *Computation of Unique Kinematic Solutions of a Spherical Parallel Manipulator with Coaxial Input Shafts*. URL: https://ieeexplore.ieee.org/document/8843090. accessed: 12.10.2024.

[6] M. Olinski, A. Gronowicz, and M. Ceccarelli. *Development and characterisation of a controllable adjustable knee joint mechanism*. URL: https://www.sciencedirect.com/science/article/pii/S0094114X20303207. (accessed: 18.10.2024).

[7] J. Wu et al. *Design and performance analysis of a novel closed-chain elastic-bionic leg with one actuated degree of freedom*. URL: https://www.sciencedirect.com/science/article/pii/S0094114X21002020. (accessed: 18.10.2024).

[8] M. Djennanel et al. *Design, Analysis, and Implementation of a 3-DOF Spherical Parallel Manipulator*. URL: https://ieeexplore.ieee.org/document/10495028. accessed: 12.10.2024.

[9] S. Phoengsongkhro et al. *Development of four-bar polycentric knee joint with stance-phase knee flexion*. URL: https://www.nature.com/articles/s41598-023-49879-4. (accessed: 21.10.2024).